Dietary obesity-associated Hif1α activation in adipocytes restricts fatty acid oxidation and energy expenditure via suppression of the Sirt2-NAD$^+$ system

Jaya Krishnan,[1,2] Carsten Danzer,[1,2] Tatiana Simka,[1,2] Josef Ukropec,[3] Katharina Manuela Walter,[1,2] Susann Kumpf,[1,2] Peter Mirtschink,[1,2] Barbara Ukropcova,[3] Daniela Gasperikova,[3] Thierry Pedrazzini,[4] and Wilhelm Krek[1,2,5]

[1]Institute of Cell Biology, [2]Competence Center for Systems Physiology and Metabolic Diseases, ETH Zurich, 8093 Zurich, Switzerland; [3]Institute of Experimental Endocrinology Slovak Academy of Sciences, Bratislava, Slovakia; [4]Department of Medicine, University of Lausanne Medical School, 1011 Lausanne, Switzerland

Dietary obesity is a major factor in the development of type 2 diabetes and is associated with intra-adipose tissue hypoxia and activation of hypoxia-inducible factor 1α (HIF1α). Here we report that, in mice, Hif1α activation in visceral white adipocytes is critical to maintain dietary obesity and associated pathologies, including glucose intolerance, insulin resistance, and cardiomyopathy. This function of Hif1α is linked to its capacity to suppress β-oxidation, in part, through transcriptional repression of *sirtuin 2* (*Sirt2*) NAD$^+$-dependent deacetylase. Reduced Sirt2 function directly translates into diminished deacetylation of PPARγ coactivator 1α (Pgc1α) and expression of β-oxidation and mitochondrial genes. Importantly, visceral adipose tissue from human obese subjects is characterized by high levels of HIF1α and low levels of SIRT2. Thus, by negatively regulating the Sirt2–Pgc1α regulatory axis, Hif1α negates adipocyte-intrinsic pathways of fatty acid catabolism, thereby creating a metabolic state supporting the development of obesity.

[*Keywords*: Hif1α; Sirt2; adipocytes; obesity; diabetes; metabolism]

Supplemental material is available for this article.

Received September 30, 2011; revised version accepted December 28, 2011.

Human obesity is characterized by enlargement of visceral white adipose tissue (WAT) mass and is associated with a greater propensity to develop type 2 diabetes, hypertension, dyslipidemia, cardiovascular diseases, and cancer (Vague 1947; Montague and O'Rahilly 2000). Visceral fat enlargement encompasses an increase in both adipocyte cell size and cell number. However, it is predominantly the increase in visceral adipocyte cell size (adipocyte hypertrophy) that is strongly influenced by diet and is linked to a greater susceptibility of developing obesity-related pathologies (Donohoe et al. 2011). Indeed, nutrient overload, a key factor in promoting the obese state, induces adipocyte hypertrophy and can promote development of insulin resistance and glucose intolerance (Kopecky et al. 2004).

Several lines of evidence suggest that visceral adipose tissue of obese human subjects and mouse models of obesity is poorly oxygenated, implying that adipose tissue expansion in response to chronic and excessive nutrient consumption creates a state of relative hypoxia due to an inability of the pre-existing adipose tissue vasculature to meet the oxygen demands of the expanding tissue (Wood et al. 2009). In mammals, decreased oxygen availability is directly connected to the activation of hypoxia-inducible factor (HIF), dimers composed of oxygen-regulated HIF1α, HIF2α, or HIF3α (collectively HIFα) and HIF1β/ARNT subunits. The ensuing induction of HIF-dependent target genes mediates the many adaptive responses to low oxygen (hypoxia), including the promotion of angiogenesis and cell survival, as well as changes in cellular metabolism (Kaelin and Ratcliffe 2008). There is evidence to suggest that among the HIFα subunits, in a context-dependent manner, HIF1α preferentially activates genes important for glycolysis, while HIF2α appears to favor the activation of genes involved in angiogenesis (Hu et al. 2003).

The reprogramming of cellular metabolism by HIF involves a switch toward increased glycolysis and free fatty acid and triacylglyceride synthesis (Krishnan et al. 2009; Wellen and Thompson 2010), implicating a central

[5]Corresponding author.
E-mail wilhelm.krek@cell.biol.ethz.ch.
Article is online at http://www.genesdev.org/cgi/doi/10.1101/gad.180406.111. Freely available online through the *Genes & Development* Open Access option.

role for HIF1α in the change of metabolic strategy following a reduction in ambient oxygen concentrations. In this regard, there is evidence to suggest that HIF1α protein accumulates in adipocytes of obese humans and mouse models of obesity (Ye 2009). While mouse models wherein HIF1α has been either overexpressed (Halberg et al. 2009), deleted in WAT (Jiang et al. 2011), or expressed as a dominant-negative form (Zhang et al. 2010) have been generated, they have not been suitable to interrogate a specific requirement of HIF1α function for maintaining the obese state (as opposed to the development of the obese state) and its associated pathologies. Hence, it remains unclear whether and how HIF1α function contributes to the maintenance of adiposity and its associated pathologies in the context of a pre-existing obese, diabetic, and cardiomyopathic state.

Here we demonstrate that Hif1α protein accumulation is restricted to adipose depots of pathologically obese and diabetic humans and mice and that this accumulation results in an inhibition of fatty acid oxidation (FAO) and energetic uncoupling via transcriptional repression of *sirtuin 2* (*Sirt2*), a member of the silent information regulator two class I (sirtuins, Sirt1–3) family of NAD^+-dependent deacetylases. Sirt2 is the most abundantly expressed family member in adipocytes and has been implicated in promoting FAO by deacetylating various substrates (Jing et al. 2007; Wang et al. 2007). In this regard, adipocyte-specific inactivation of *Hif1α* in obese mice induces the accumulation of nuclear Sirt2 and an attendant reduction of acetylation of the transcriptional coactivator PPARγ coactivator 1α (Pgc1α). We propose that the negative effects of Hif1α on the sirtuin–Pgc1α metabolic regulatory system contributes to the suppression of genes involved in promoting energy expenditure and fatty acid catabolism. Therefore, our data assign a key role for Hif1α in the promotion and maintenance of dietary obesity and suggest that these effects are brought about, at least in part, by suppressing adipocyte lipid catabolism.

Results

Adipocyte-specific Hif1α inactivation attenuates dietary-driven adipose tissue expansion and its associated pathologies

Nutrient overload facilitates adipose mass expansion and the development of intra-adipose hypoxia, culminating in Hif1α accumulation in visceral adipocytes (Ye et al. 2007). To define the functional relevance of nutrient overload-induced adipocyte Hif1α accumulation in adult mice, we crossed Hif1α f/f mice with aP2-Cre-ERT2 mice bearing *Cre recombinase* under the control of the tamoxifen-inducible aP2 promoter (hereafter referred to as Hif1α icKO) (Imai et al. 2001). Littermates lacking the aP2-Cre-ERT2 transgene are termed Hif1α iC. This model permits the specific interrogation of Hif1α function in adult adipocytes and circumvents the problem of non-adipocyte Cre activation during embryogenesis and in early postnatal development that has been shown to occur in the constitutive, noninducble aP2-cre recombinase mouse line (Urs et al. 2006; Martens et al. 2010). Therefore, the aP2-Cre-ERT2 model enables uncoupling of adipocyte-intrinsic consequences of gene inactivation from that due to altered adipose tissue inflammation that occurs in response to nutritional overload (Imai et al. 2001).

Hif1α iC and Hif1α icKO mice were placed on either a normal chow diet (NCD) (Fig. 1A, top panel) or a high-fat diet (HFD) (Fig. 1A, bottom panel) protocol at 4 wk of age for a period of 18 wk, at which time Hif1α was excised by tamoxifen-induced Cre activation (Fig. 1A). Hif1α iC and Hif1α icKO mice administered with tamoxifen are termed Hif1α iC(T) and Hif1α icKO(T), respectively. Hif1α iC(T) and Hif1α icKO(T) mice were maintained on NCD or HFD thereafter (referred to as the NCD/NCD or HFD/HFD protocol, respectively). Tamoxifen delivery led to a robust reduction in Hif1α mRNA specifically in WAT and brown adipose tissue (BAT) of mice maintained on the NCD/NCD or HFD/HFD protocols (Fig. 1B). Hif1α mRNA levels were unaltered in nonadipose tissues (Supplemental Material; Supplemental Fig. 1A,B), and genomic excision at the floxed Hif1α locus was not observed (data not shown). Strikingly, Hif1α inactivation led to a decrease in visceral white adipocyte cell size in mice maintained on the HFD/HFD protocol 13 wk post-tamoxifen delivery (Fig. 1C) in the absence of changes in white adipocyte cell number (data not shown). Excision of Hif1α in BAT, however, had negligible effects on either brown adipocyte cell size (Fig. 1C) or cell number (data not shown). Additionally, lipid content of Hif1α icKO(T) visceral white adipocytes, as indicated by boron-dipyrromethene (BODIPY) incorporation, was significantly diminished compared with Hif1α iC(T)-derived white adipocytes maintained on HFD/HFD (Fig. 3E, below; Supplemental Material; Supplemental Fig. 3A).

Prior to the inactivation of Hif1α by tamoxifen, NCD/NCD and HFD/HFD mice displayed a similar increase in body mass, regardless of the *Cre recombinase* transgene status (Fig. 1D). Following tamoxifen-induced Hif1α excision at week 18, Hif1α icKO(T) mice of the HFD/HFD group gained significantly less weight compared with control Hif1α iC(T) mice (Fig. 1D). In contrast, Hif1α iC(T) and Hif1α icKO(T) mice maintained on the NCD/NCD protocol showed comparable weight gain throughout, despite being similarly treated with tamoxifen at week 18 (Fig. 1D). Organs harvested from Hif1α icKO(T) mice maintained on NCD/NCD at 13 wk post-Hif1α excision revealed an ~10%–15% reduction in visceral WAT, while other organs analyzed were of a weight comparable with that of Hif1α iC(T) mice (Fig. 1E). However, at 13 wk post-Hif1α excision, Hif1α icKO(T) mice maintained on the HFD/HFD protocol exhibited a dramatic reduction in overall visceral WAT compared with Hif1α iC(T) littermates maintained on the HFD/HFD protocol (Fig. 1F). All other organs analyzed were of a weight comparable with control mice maintained on NCD/NCD (Fig. 1E,F). It should be noted that control mice maintained on the HFD/HFD protocol displayed an increase in liver mass that was less obvious in Hif1α icKO(T) mice post-Hif1α excision (Fig. 1F) and is likely

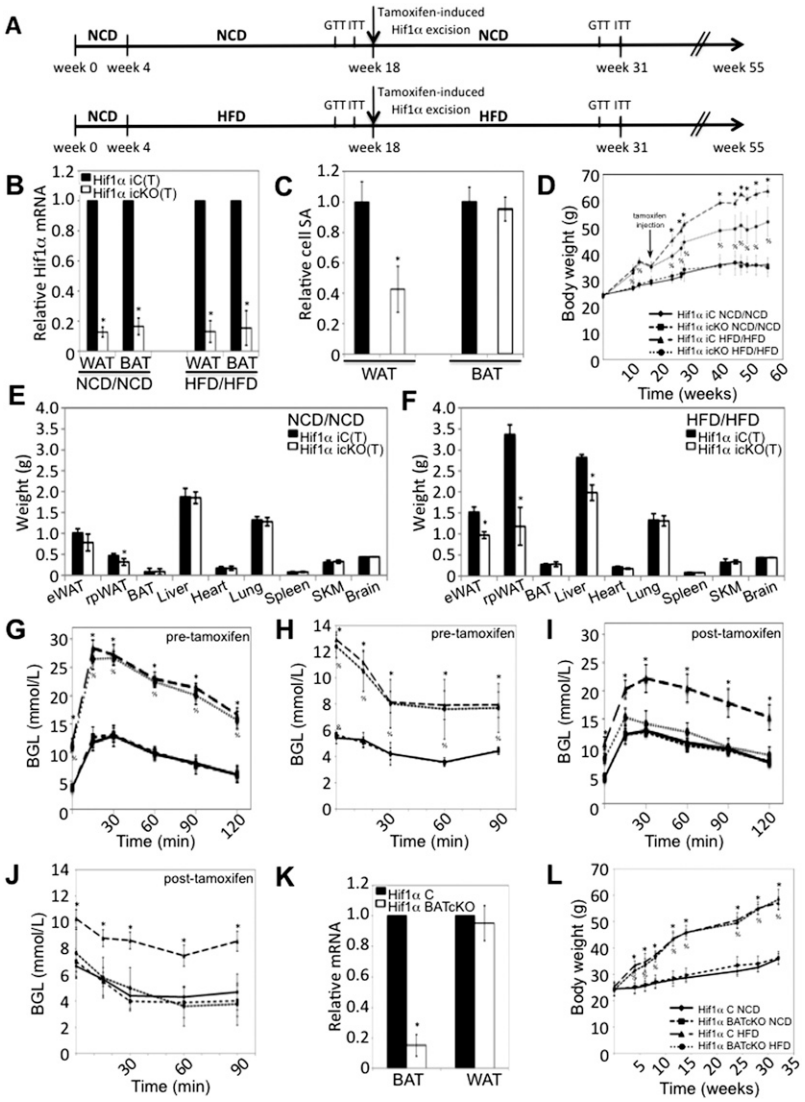

Figure 1. Temporal Hif1α inactivation attenuates adipose tissue expansion and protects from obesity-associated pathologies. (*A*) Schematic representation of the NCD/NCD (*top* panel) and HFD/HFD (*bottom* panel) protocols. All Hif1α iC and Hif1α icKO mice were initially maintained on a NCD to 4 wk of age, after which, Hif1α iC and Hif1α icKO littermates were randomly assigned to either the NCD/NCD or HFD/HFD protocol. NCD/NCD and HFD/HFD mice were maintained on a NCD or HFD for 14 wk thereafter, and tamoxifen was administered to both Hif1α iC and Hif1α icKO mice. The mice were maintained on either the NCD or HFD feeding protocol, respectively, following tamoxifen administration. GTT and ITT measurements were taken prior to Hif1α inactivation at weeks 16 and 17, respectively, and at weeks 14 and 15 post-Hif1α inactivation, respectively. (*B*) Visceral WAT and intrascapular BAT biopsies of tamoxifen-induced NCD/NCD- and HFD/HFD-maintained Hif1α iC(T) and Hif1α icKO(T) mice were assessed for Hif1α mRNA expression by qPCR. All values were normalized internally to 18S RNA expression and to the Hif1α iC(T) control, respectively. (⋆) $P < 0.01$ versus control, set at 1.0. Data are mean ± SEM of values from five mice per group. (*C*) Visceral WAT and BAT sections of Hif1α iC(T) and Hif1α icKO(T) mice maintained on the HFD/HFD protocol for 16 wk post-tamoxifen induction were stained with phalloidin to mark actin and the cell periphery and counterstained with DAPI. Confocal microscopic imaging was performed, and the cell surface area was quantified. Surface area measurements relative to Hif1α iC(T) sections are shown, which was set at 1.0. (⋆) $P < 0.01$. Data are mean ± SEM of values from five mice per group. (*D*) Hif1α iC(T) ($n = 8$ NCD/NCD; $n = 10$ HFD/HFD) and Hif1α icKO(T) ($n = 7$ NCD/NCD; $n = 12$ HFD/HFD) mice were assessed for changes in body weight at the indicated time points. (⋆) $P < 0.05$ versus Hif1α iC(T) HFD/HFD; (%) $P < 0.05$ versus Hif1α iC(T) NCD/NCD and Hif1α icKO(T) NCD/NCD. Data are mean ± SEM of values from each group. (*E*,*F*) Individual organs of Hif1α iC(T) ($n = 8$ NCD/NCD; $n = 10$ HFD/HFD) and Hif1α icKO(T) ($n = 7$ NCD/NCD; $n = 12$ HFD/HFD) mice were excised and weighed 16 wk post-tamoxifen induction. eWAT, rpWAT, and SKM indicate epididymal WAT, retroperitoneal WAT, and skeletal muscle, respectively. (⋆) $P < 0.05$ versus Hif1α iC(T). Data are mean ± SEM of values from each group. (*G*) GTT measurements of Hif1α iC(T) ($n = 8$ NCD/NCD; $n = 10$ HFD/HFD) and Hif1α icKO(T) ($n = 7$ NCD/NCD; $n = 12$ HFD/HFD) mice prior to tamoxifen-mediated Hif1α excision at week 16. (⋆,%) $P < 0.05$ versus Hif1α iC(T) NCD/NCD. Data are mean ± SEM of values from each group. (*H*) ITT measurements of Hif1α iC(T) ($n = 8$ NCD/NCD; $n = 10$ HFD/HFD) and Hif1α icKO(T) ($n = 7$ NCD/NCD; $n = 12$ HFD/HFD) mice prior to tamoxifen-mediated Hif1α excision at week 17. (⋆,%) $P < 0.05$ versus Hif1α iC(T) NCD/NCD. Data are mean ± SEM of values from each group. (*I*) GTT measurements of Hif1α iC(T) ($n = 8$ NCD/NCD; $n = 10$ HFD/HFD) and Hif1α icKO(T) ($n = 7$ NCD/NCD; $n = 12$ HFD/HFD) mice at 16 wk post-tamoxifen-mediated Hif1α excision. (⋆,%) $P < 0.05$ versus Hif1α iC(T) NCD/NCD. Data are mean ± SEM of values from each group. (*J*) ITT measurements of Hif1α iC(T) ($n = 8$ NCD/NCD; $n = 10$ HFD/HFD) and Hif1α icKO(T) ($n = 7$ NCD/NCD; $n = 12$ HFD/HFD) mice at 17 wk post-tamoxifen-mediated Hif1α excision. (⋆) $P < 0.05$ versus Hif1α iC(T) NCD/NCD. Data are mean ± SEM of values from each group. (*K*) Intrascapular BAT and visceral WAT biopsies of Hif1α C and Hif1α BATcKO mice maintained on either NCD or HFD were assessed for Hif1α mRNA expression by qPCR. All values were normalized internally to 18S RNA expression and to the Hif1α C control. (⋆) $P < 0.01$ versus control, set at 1.0. Data are mean ± SEM of values from seven mice per group. (*L*) Hif1α f/f ($n = 10$ NCD; $n = 12$ HFD) and Hif1α BATcKO ($n = 8$ NCD; $n = 12$ HFD) mice were maintained on either a NCD or HFD. Body weight measurements were taken at the indicated time points throughout the course of the protocol. (⋆,%) $P < 0.05$ versus NCD group. Data are mean ± SEM of values from each group.

a consequence of nutrient-overload-induced liver steatosis (Buettner et al. 2006). To determine whether excess nutrients were being redistributed toward muscle or nonadipose tissue growth in Hif1α icKO(T) mice, we assessed lean body mass of HFD/HFD Hif1α iC(T) and Hif1α icKO(T) mice at 16 wk post-tamoxifen induction by carcass analy-

sis. As shown in the Supplemental Material (Supplemental Fig. 1C), total lean mass was comparable between the respective lines on either dietary protocol, implying that nutrient rechanneling to nonadipose tissue did not occur to a measurable extent.

To address the impact of adipocyte-specific Hif1α inactivation on systemic glucose homeostasis, Hif1α iC(T) and Hif1α icKO(T) mice of the NCD/NCD and HFD/HFD groups were subjected to a glucose tolerance test (GTT) and insulin tolerance test (ITT) prior to and post-tamoxifen-mediated Hif1α excision. Hif1α iC(T) and Hif1α icKO(T) maintained on the NCD/NCD protocol exhibited a comparable response to glucose and insulin both prior to and post-tamoxifen-mediated Hif1α excision (Fig. 1G–J). In contrast, while Hif1α iC(T) and Hif1α icKO(T) maintained on HFD/HFD exhibited comparable glucose tolerance and insulin sensitivity prior to Hif1α excision (Fig. 1G,H), GTT and ITT measurements performed post-Hif1α excision unveiled a significant improvement in glucose tolerance and peripheral insulin sensitivity in Hif1α icKO(T) mice (Fig. 1I,J).

Diabetic cardiomyopathy is a complication commonly associated with obesity. It is characterized by epicardial fat accumulation, steatosis, cardiac dilatation, and contractile dysfunction (Boudina and Abel 2010). Although Hif1α iC and Hif1α icKO mice maintained on the HFD/HFD protocol exhibited reduced cardiac contractility at week 18 (prior to Hif1α excision), as indicated by the decrease in cardiac fractional shortening, the inactivation of Hif1α led to a gradual normalization of cardiac function that was not observed in control mice (Supplemental Material; Supplemental Fig. 1D). Additionally, Hif1α icKO(T) mice displayed reduced left ventricular dilation and decreased epicardial fat accumulation compared with control mice (Supplemental Material; Supplemental Fig. 1E,F). Importantly, Cre recombinase activity was not detected in the hearts of Hif1α iC(T) or Hif1α icKO(T) mice (Supplemental Material; Supplemental Fig. 1A,B).

The results above prompted us to address whether Hif1α inactivation would similarly inhibit weight gain in HFD-induced obese mice when transferred to a NCD. To that end, Hif1α iC and Hif1α icKO mice were maintained initially on a HFD for 18 wk and, following tamoxifen-mediated Hif1α inactivation, were placed on an NCD (HFD/NCD protocol) (Supplemental Material; Supplemental Fig. 1G, bottom panel). Hif1α iC and Hif1α icKO maintained throughout on a NCD serve as controls (Supplemental Material; Supplemental Fig. 1G, top panel). When obese mice were switched to a NCD post-tamoxifen treatment, both Hif1α iC(T) and Hif1α icKO(T) mice began losing weight. However, Hif1α icKO(T) mice exhibited expedited weight loss compared with controls (Supplemental Material; Supplemental Fig. 1H). Strikingly, by week 23 post-tamoxifen treatment, Hif1α icKO(T) maintained on the HFD/NCD protocol displayed body weight comparable with mice maintained on a NCD throughout (i.e., NCD/NCD protocol) (Supplemental Material; Supplemental Fig. 1H). Although Hif1α iC and Hif1α icKO responded similarly to a glucose challenge while on a HFD prior to tamoxifen induction (Supplemental Material; Supplemental Fig. 1I), Hif1α icKO(T) mice displayed a time-dependent accelerated improvement in glucose tolerance compared with the littermate Hif1α iC(T) post-tamoxifen treatment (Supplemental Material; Supplemental Fig. 1J,K). The presence of the *Cre recombinase* transgene alone or in combination with tamoxifen treatment does not confer a discernible phenotype in the background of wild-type Hif1α alleles (data not shown). Additionally, in the absence of tamoxifen treatment, Hif1α icKO mice are indistinguishable from littermate Hif1α iC mice when maintained on a long-term NCD, HFD, or HFD/NCD protocol (data not shown). These results corroborate a critical requirement for Hif1α function in maintaining dietary obesity and its associated pathologies.

To uncouple the effects of Hif1α inactivation in WAT as opposed to BAT on adiposity, mice lacking Hif1α specifically in BAT were generated by crossing Hif1α f/f mice with mice harboring the *Cre recombinase* transgene under the control of the brown adipocyte-specific uncoupling protein 1 (UCP1) promoter (Guerra et al. 2001). Hif1α f/f mice carrying the UCP1-Cre recombinase transgene are termed Hif1α BATcKO, while their corresponding littermates lacking the UCP1 driven-Cre recombinase transgene are termed Hif1α C. The Hif1α floxed allele was efficiently excised specifically in BAT (Fig. 1K). However, BAT-specific Hif1α inactivation did not impact BAT or WAT weight (Supplemental Material; Supplemental Fig. 1L,M) or alter brown adipocyte morphology or BAT gene expression (data not shown). To determine whether the loss of Hif1α in BAT would affect weight gain, Hif1α C and Hif1α BATcKO mice were placed on a long-term NCD or HFD protocol. Intriguingly, BAT-specific Hif1α inactivation did not affect WAT expansion (data not shown) or weight gain in mice when maintained on either chow or HFD (Fig. 1L).

Adipose-specific Hif1α inactivation promotes β-oxidation and energy expenditure

Caloric intake and energy homeostasis are critical parameters in WAT mass regulation (North and Verdin 2004). As Hif1α iC(T) and Hif1α icKO(T) mice on the HFD/HFD protocol had a comparable food intake (Fig. 2A; Supplemental Material; Supplemental Fig. 2A), we addressed whether the inactivation of Hif1α in adipocytes affected energy expenditure by indirect calorimetry. Hif1α iC(T) and Hif1α icKO(T) mice maintained on a HFD/HFD protocol were placed in metabolic cages at 15 wk post-Hif1α excision and assessed for oxygen consumption, resting energy expenditure (REE) (through application of Weir's formula) (van der Kuip et al. 2004), and, in parallel, basal body temperature. Hif1α icKO(T) mice exhibited a greater degree of oxygen consumption and energy expenditure, as evidenced by increased REE and body temperature compared with Hif1α iC(T) mice (Fig. 2B–D). This was paralleled by an increase in carbon dioxide expiration (Fig. 2E). The respiratory exchange ratio (RER) gives an indication of preferential carbohydrate or fatty acid catabolism (Nunn 1972). As shown in Figure 2F, Hif1α icKO(T) mice dem-

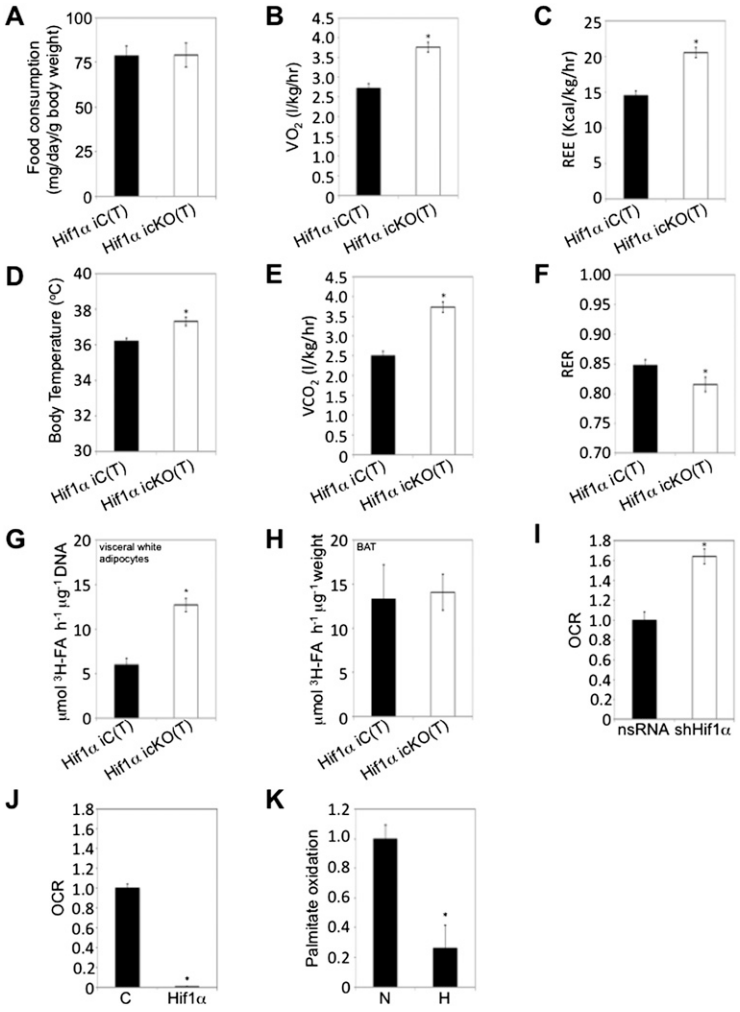

Figure 2. Visceral adipose Hif1α inactivation promotes fatty acid β-oxidation and systemic energy expenditure. (*A*) Individually housed Hif1α iC(T) (n = 10) and Hif1α icKO(T) (n = 12) mice maintained on a HFD/HFD protocol were assessed for food intake over a period of 3 wk (between weeks 12–15 post-tamoxifen administration). Data are mean ± SEM of values from each group. (*B–F*) Hif1α iC(T) and Hif1α icKO(T) mice subjected to the HFD/HFD protocol were placed in metabolic cages at 15 wk post-Hif1α inactivation. Resting O_2 consumption (*B*), energy expenditure (*C*), body temperature (*D*), CO_2 expiration (*E*), and RER (*F*) measurements are shown. (*) $P < 0.01$ versus Hif1α iC(T) HFD/HFD. Data are mean ± SEM of values from six mice per group. (*G,H*) Primary visceral white adipocytes (*G*) and BAT explants (*H*) isolated from Hif1α iC(T) and Hif1α icKO(T) mice maintained on the HFD/HFD protocol were assessed for palmitate oxidation. (*) $P < 0.05$ veruss Hif1α iC(T) HFD/HFD. Data are mean ± SEM of values from four mice per group. (*I,J*) 3T3-L1-derived adipocytes were infected with shHif1α-encoding viruses or the corresponding nsRNA control (*I*), empty (mock, *C*), or Hif1α-encoding (*J*) virus and assessed for oleate-induced oxygen consumption rate (OCR) as a measure of fatty acid β-oxidation using the Seahorse Bioscience 24XF extracellular flux analyzer. (*) $P < 0.01$ compared with control, set at 1.0. Data are mean ± SEM of values from each group. (*K*) Differentiated 3T3-L1 adipocytes were cultured in normoxia (N, 20% O_2) or hypoxia (H, 3% O_2) and assessed for palmitate oxidation. (*) $P < 0.01$ compared with normoxia control (N), set at 1.0. Data are mean ± SEM of values from each group.

onstrated a greater degree of FAO compared with Hif1α icKO(T) mice. These observations suggest that Hif1α deficiency prevents WAT expansion, at least in part, by permitting increased FAO in adipose tissue.

To determine whether the increase in FAO upon HIF1α deletion at the organismal level could be ascribed to a specific adipose depot, visceral and subcutaneous white adipocytes and BAT from the respective mice were assessed for palmitate oxidation (Fig. 2G,H; Supplemental Material; Supplemental Fig. 2B). Surprisingly, BAT and subcutaneous white adipocytes derived from Hif1α icKO(T) exhibited levels of palmitate oxidation similar to those of Hif1α iC(T) mice. In contrast, visceral white adipocytes of HFD/HFD mice lacking Hif1α displayed increased palmitate oxidation compared with controls (Fig. 2G). Differences in palmitate oxidation were not observed in visceral adipocytes of mice maintained on NCD/NCD (Supplemental Material; Supplemental Fig. 2C). These observations imply that loss of Hif1α function is associated with increased FAO selectively in visceral white adipocytes.

Consistent with these data, quantitative PCR (qPCR) analysis of visceral WAT depots of Hif1α icKO(T) mice revealed a general increase in expression of fatty acid catabolic enzymes compared with Hif1α iC(T) mice (Supplemental Material; Supplemental Fig. 2D). In contrast, subcutaneous fat depots of Hif1α iC(T) and Hif1α icKO(T) did not reveal significant differences in expression of FAO regulators (Supplemental Material; Supplemental Fig. 2E,F). To corroborate these data, preadipocytes were harvested from the subcutaneous and visceral fat depots of Hif1α iC(T) and Hif1α icKO(T) mice maintained on a HFD/HFD protocol and induced to differentiate in vitro. Thereafter, oleate-induced oxygen consumption, as a measure of fatty acid β-oxidation, was assessed using the Seahorse Bioscience 24XF extracellular flux analyzer (Supplemental Material; Supplemental Fig. 2G,H). While subcutaneous preadipocyte-derived cells exhibited similar levels of FAO regardless of Hif1α status (Supplemental Material; Supplemental Fig. 2H), visceral preadipocyte-derived cells of Hif1α icKO(T) mice showed increased FAO capacity compared with Hif1α iC(T) visceral adipocytes (Supplemental Material; Supplemental Fig. 2G).

The fact that adipocyte Hif1α inactivation predominantly promotes visceral FAO led us to examine the effect of dietary obesity on the depot-specific FAO capacity of wild-type C57/Bl6 mice. C57/Bl6 mice were maintained

on NCD or HFD for 20 wk. HFD-maintained mice displayed an increase in body weight compared with NCD mice and repression of visceral WAT FAO capacity (Supplemental Material; Supplemental Fig. 2I,J). Strikingly, subcutaneous FAO capacity remained largely unaltered in mice fed with either a NCD or HFD (Supplemental Material; Supplemental Fig. 2J), implying a specific role for Hif1α in mediating suppression of FAO capacity in visceral WAT during dietary-induced obesity. Consistent with these observations, increased Hif1α protein accumulation and target gene expression were observed primarily in visceral WAT of mice maintained on HFD (Supplemental Material; Supplemental Fig. 2K–N).

To ascertain the cell autonomy of Hif1α function in adipocyte FAO regulation, 3T3-L1 preadipocytes that can be differentiated to form mature adipocytes were used. Although Hif1α has been linked to inhibition of preadipocyte differentiation, its activity is restricted to the earliest stages of differentiation (at 3–6 h post-differentiation) and precedes the expression of PPARγ (Imagawa et al. 1999). We validated that our 3T3-L1 differentiation protocol consistently led to mature adipocytes by day 4 using the expression of Pparγ, C/ebpα, and Fasn, and lipid droplet accumulation as readout for mature adipocyte formation (data not shown). In this setting, Hif1α was then either down-regulated or ectopically expressed at day 4 post-differentiation using lentiviruses carrying shRNAs targeting Hif1α mRNA (shHif1α) or expressing exogenous Hif1α. While lentiviral expression of shHif1α led to an increase in oxygen consumption using the Seahorse Bioscience 24XF extracellular flux analyzer (Fig. 2I), ectopic expression of Hif1α completely abolished the oleate-oxidizing capacity of 3T3-L1-derived adipocytes (Fig. 2J). Lentiviral expression of nonsilencing shRNAs (nsRNA) or of an empty expression cassette served as controls. Immunoblotting confirmed ectopic expression of Hif1α or its depletion in these experiments (Fig. 4E, below, bottom panel). In addition, we assessed the effects of hypoxia (3% O_2) on palmitate oxidation as well as the expression of mitochondrial biogenesis and FAO genes in differentiated 3T3-L1 adipocytes. Similar to ectopic Hif1α expression (Fig. 2J; Supplemental Material; Supplemental Fig. 2O), hypoxia led to the suppression of palmitate oxidation and multiple mitochondrial and FAO genes (Supplemental Material; Supplemental Fig. 2O,P). Together, these data suggest a role for Hif1α in the negative regulation of white adipocyte FAO capacity.

Hif1α inactivation promotes mitochondrial biogenesis specifically in white adipocytes

Upon characterizing gene expression changes affected by Hif1α inactivation in WAT, we observed an increase in the expression of the nuclear-encoded transcriptional inducers of mitochondrial biogenesis nuclear respiratory factor 1 (Nrf1) and estrogen-related receptor 1β (Err1β) and of the mitochondrial-encoded transcription factor A (Tfam) and transcription factor B2 (Tfb2m) (Fig. 3A). Components

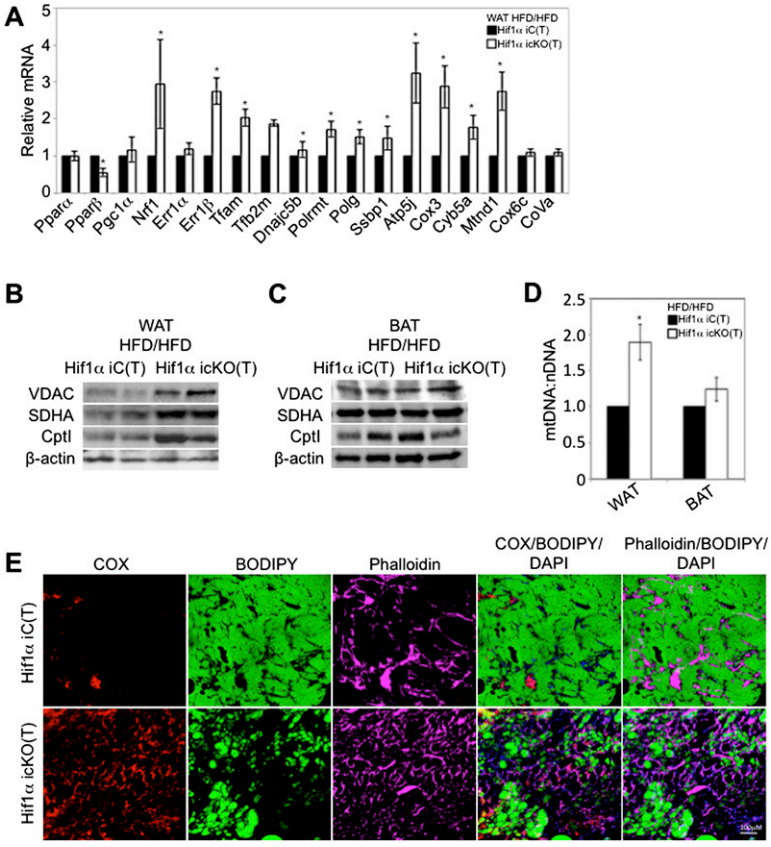

Figure 3. Hif1α inactivation in visceral WAT promotes Pgc1α target gene expression and mitochondrial biogenesis. (*A*) Gene expression profiling of visceral WAT of Hif1α iC(T) and Hif1α icKO(T) mice maintained on the HFD/HFD protocol for regulators FAO and mitochondrial biogenesis. All values were normalized internally to 18S RNA expression and to the Hif1α iC(T) control, respectively. (*) $P < 0.01$ compared with control, set at 1.0. Data are mean ± SEM of values from five mice per group. (*B*,*C*) Visceral WAT (*B*) and BAT (*C*) biopsies of Hif1α iC(T) and Hif1α icKO(T) maintained on the HFD/HFD protocol were probed for protein expression of VDAC, SDHA, and Cpt1. Sample loading was normalized to β-actin. (*D*) Quantification of mitochondrial DNA content relative to nuclear DNA content in visceral WAT and BAT. All values were normalized to the Hif1α iC(T) control, respectively. (*) $P < 0.05$ compared with control, set at 1.0. Data are mean ± SEM of values from four to five mice per group. (*E*) Visceral WAT sections of Hif1α iC(T) and Hif1α icKO(T) mice maintained on the HFD/HFD protocol were stained for the mitochondrial marker cytochrome oxidase (COX, red), BODIPY (green), phalloidin (pink), and DAPI (blue) and analyzed by immunofluorescence confocal microscopy.

of the mitochondrial DNA replication and transcription machinery, including ssDNA-binding protein 1 (Ssbp1) and mitochondrial DNA-directed RNA polymerases Polrmt and Polg, were similarly up-regulated, concomitant with the increased expression of components of oxidative phosphorylation and of the mitochondrial electron transport chain, such as reduced nicotinamide adenine dinucleotide (NADH)–ubiquinone oxidoreductase subunit 1 (Mtnd1) and cytochrome c oxidase subunit III (Cox3) (Fig. 3A).

As Hif1α inactivation resulted in increased expression of mitochondrial biogenesis modulators, we asked whether WAT lacking Hif1α exhibited increased mitochondrial content. Retroperitoneal WAT protein lysates from Hif1α iC(T) and Hif1α icKO(T) mice were probed for expression of the mitochondrial markers' voltage-dependent anion channel (VDAC) and succinate dehydrogenase complex subunit A (SDHA) by immunoblotting. Indeed, as shown in Figure 3B, increased VDAC and SDHA protein was observed specifically in WAT of Hif1α icKO(T) mice but not Hif1α iC(T) mice. Importantly, VDAC and SDHA protein levels were comparable between BAT of Hif1α iC(T) and Hif1α icKO(T) mice (Fig. 3C). Quantification of mitochondrial DNA content confirmed the relative increase in mitochondrial content in Hif1α icKO(T) white adipocytes compared with controls (Fig. 3D). BAT mitochondrial content was unaffected by Hif1α status (Fig. 3D). Immunofluorescence imaging of visceral WAT biopsies probed for the mitochondrial marker cytochrome oxidase (COX) revealed an increase in mitochondrial number in biopsies lacking Hif1α. The increase in mitochondrial number paralleled a decrease in BODIPY incorporation (Fig. 3E). Higher-magnification images of the panels displayed in Figure 3E suggest that the mitochondrial staining in visceral WAT biopsies of control Hif1α iC(T) is largely restricted to the nonadipocyte population (Supplemental Material; Supplemental Fig. 3A). Taken together, these data suggest a critical role for Hif1α in the regulation of white, but not brown, adipocyte mitochondrial biogenesis.

Hif1α regulates Pgc1α acetylation state via Sirt2 *transcriptional repression*

Pgc1α is a transcriptional coactivator important for oxidative catabolism, mitochondrial biogenesis, and energy expenditure (Wu et al. 1999). Although Pgc1α mRNA and protein levels were unaffected by Hif1α inactivation (Fig. 3A), the gene expression profile and cellular phenotype of WAT lacking Hif1α were characteristic of increased Pgc1α-mediated transcription. In this regard, the activity of established Pgc1α-responsive promoter-luciferase reporters—namely, those of Cox3, Cpt1, and PEPCK (Rodgers et al. 2005)—was increased in Hif1α-depleted 3T3-L1 adipocytes (Supplemental Material; Supplemental Fig. 4A–C), implying that Pgc1α function may be affected.

The acetylation state of Pgc1α is known to be a critical determinant of its transcriptional coactivation function (Rodgers et al. 2005). Hence, we addressed whether the inactivation of Hif1α could impact the Pgc1α acetylation state. Indeed, immunoprecipitates of Pgc1α from WAT of Hif1α iC(T) mice maintained on a HFD/HFD protocol contained abundant acetylated Pgc1α, as evidenced by immunoblotting for acetyl-lysine (Fig. 4B). No such signal was detected in immunoprecipitates of Pgc1α from WAT of Hif1α icKO(T) mice (Fig. 4B). Given the above-noted results, we asked whether Pgc1α acetylation changes as a function of hypoxia in a Hif1α-dependent manner. As shown in the Supplemental Material (Supplemental Fig. 4D), exposure of 3T3-L1-derived adipocytes depleted for Hif1α to hypoxia led to a substantial reduction of Pgc1α acetylation compared with control. Conversely, chemical inducers of Hif1α stabilization led to increased levels of acetylated Pgc1α (Supplemental Material; Supplemental Fig. 4E).

Sirtuins are NAD^+-dependent deacetylases involved in the regulation of transcriptional responses (North et al. 2003). Examination of the mRNA expression of all known sirtuins (Sirt1–Sirt7) in WAT biopsies of Hif1α iC(T) and Hif1α icKO(T) mice maintained on the HFD/HFD revealed that, except for Sirt2, no changes in mRNA levels were observed as a function of Hif1α status (Fig. 4C,D; Supplemental Material; Supplemental Fig. 4F). The increase in Sirt2 expression was selectively evident in WAT biopsies of Hif1α icKO(T) mice maintained on the HFD/HFD protocol, as evidenced by immunoblotting and immunofluorescence confocal microscopy (Fig. 4D; Supplemental Material; Supplemental Fig. 4G), and not in WAT biopsies of mice maintained on NCD/NCD (Fig. 4C).

Sirt2 was originally identified as a tubulin deacetylase and was described to shuttle between the cytoplasm and the nucleus (North et al. 2003; Black et al. 2008). In accord with these findings, Sirt2 localized in the cytoplasm but also prominently in the nucleus of Hif1α icKO(T) visceral adipocytes (Supplemental Material; Supplemental Fig. 4G,H), a finding further supported by cell fractionation experiments (Supplemental Material; Supplemental Fig. 4H). The up-regulation of Sirt2 expression in visceral adipocytes in Hif1α icKO(T) mice correlated with decreased acetylation of the cytoplasmic Sirt2 target protein tubulin (Fig. 4D, bottom panel). Similarly, depletion of Hif1α in 3T3-L1 caused induction of Sirt2 mRNA and protein and reduced levels of acetylated tubulin (Fig. 4E). Inverse effects were seen when Hif1α was overexpressed in these cells (Fig. 4E). In contrast, Sirt1 mRNA and protein levels remained unaffected by Hif1α status (Fig. 4E). Together, these results suggest that inactivation of Hif1α is associated with increased Sirt2 mRNA and protein expression in WAT, visceral, and 3T3-L1-derived adipocytes.

To define potential mechansims underlying this phenomenon, in silico analysis of the Sirt2 promoter led to the identification of a cross-species conserved hypoxia response element (HRE) at −537 base pairs (bp) downstream from the mouse Sirt2 transcription start site (TSS) (Fig. 4F). Intriguingly, chromatin immunoprecipitation (ChIP) assays on nuclear extracts derived from adipose tissue of Hif1α iC(T) or Hif1α icKO(T) mice maintained on a HFD/HFD protocol demonstrated the interaction of Hif1α and its heterodimerization partner, Hif1β/ARNT, with the conserved HRE in the Sirt2 promoter in vivo (Fig. 4G). Luciferase reporter assays performed with the

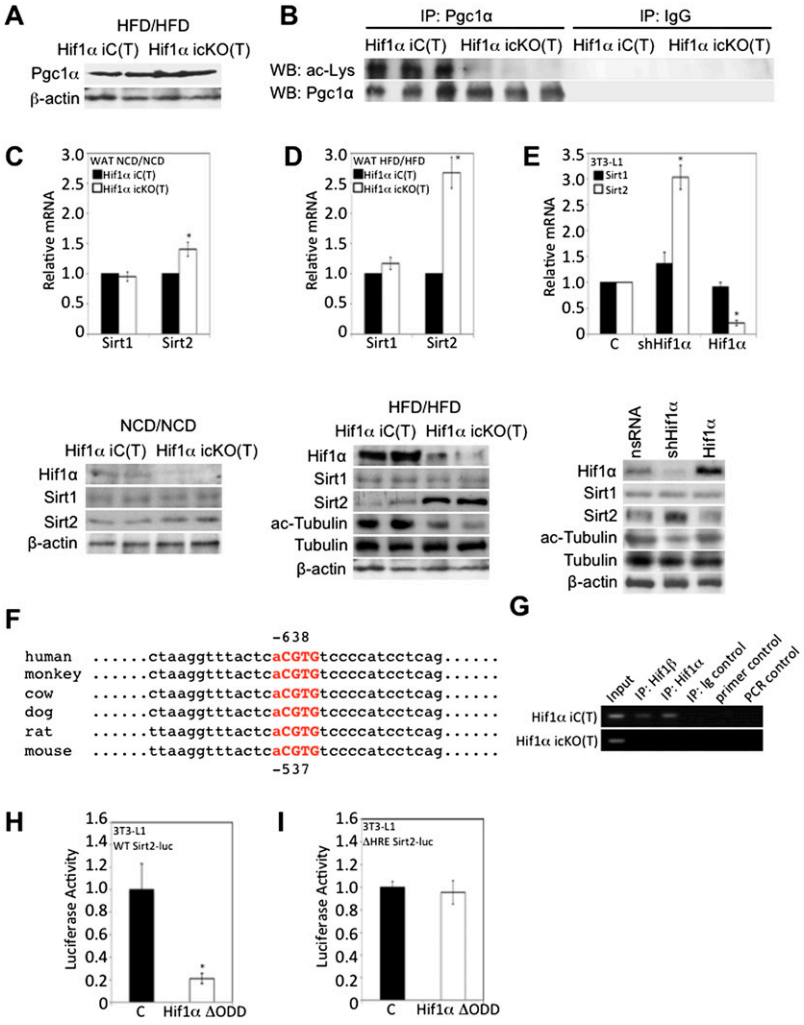

Figure 4. Hif1α inactivation promotes Pgc1α deacetylation via Sirt2. (*A*) Visceral WAT of Hif1α iC(T) and Hif1α icKO(T) mice subjected to the HFD/HFD protocol were assessed for Pgc1α protein expression. β-Actin served as a loading control. (*B*) Endogenous Pgc1α was immunoprecipitated from HFD/HFD-maintained Hif1α iC(*T*) and Hif1α icKO(T) visceral WAT lysates and probed by immunoblotting for acetylated lysine and Pgc1α. IgG antibodies were used as negative controls. (*C*,*D*) Gene expression profiling of Hif1α iC(T) and Hif1α icKO(T) mice subjected to the NFD/NFD (*D*, *top* panel) or HFD/HFD (*E*, *top* panel) protocol for Sirt1 and Sirt2 mRNA. All values were normalized internally to 18S RNA expression and to the Hif1α iC(T) control, respectively. (*) $P < 0.01$ compared with control, set at 1.0. Data are mean ± SEM of values from four mice per group. Visceral WAT of Hif1α iC(T) and Hif1α icKO(T) mice subjected to the NCD/NCD (*D*, *bottom* panel) or HFD/HFD (*E*, *bottom* panel) protocol were assessed for Hif1α, Sirt1, and Sirt2 protein expression (*C*,*D*) and tubulin acetylation (*D*). β-Actin served as a loading control. (*E*) 3T3-L1-derived adipocytes were infected with nsRNA, shHif1α, or Hif1α virus and assessed for Sirt1 and Sirt2 mRNA levels (*top* panel) and protein expression of Hif1α, Sirt1, Sirt2, and tubulin acetylation (*bottom* panel), with β-actin as a loading control. All qPCR values were normalized internally to 18S RNA expression and to nsRNA values, respectively. (*) $P < 0.01$ compared with control, set at 1.0. Data are mean ± SEM of values from each group. (*F*) Sequence analysis of the human, monkey, cow, dog, rat, and mouse Sirt2 promoters showing conserved putative HREs (in bold and red). The core consensus HRE motif is capitalized. (*G*) Hif1α iC(T) and Hif1α icKO(T) WAT derived from mice subjected to the HFD/HFD protocol were assessed for interaction of Hif1α and Hif1β at the Sirt2 promoter by ChIP. DNA from the respective samples was immunoprecipitated with a Hif1α (IP:Hif1α)-specific and a Hif1β (IP:Hif1β)-specific antibody or with a control isotype-matched antibody (IP:Ig control). Primer control and PCR control refer to reactions performed in the absence of primers or in the absence of DNA input, respectively. (*H*,*I*) Sirt2 promoter activity in response to Hif1α was determined by transient cotransfection of wild-type (WT) (*H*) and HRE-mutated (ΔHRE) (*I*) Sirt2 promoter, respectively, fused to luciferase and with either an empty vector control or a Hif1α ΔODD expression construct. All transfections contained equal amounts of a β-galactosidase expression vector for normalization of luciferase activity. (*) $P < 0.01$ compared with control, set at 1.0. Data are mean ± SEM of values from each group.

wild-type Sirt2 promoter or a mutant derivative lacking the conserved HRE (referred to as ΔHRE), upon expression of a constitutively active Hif1α mutant (Hif1α ΔODD) that escapes pVHL-mediated degradation through the deletion of the oxygen-dependent degradation domain (ODD) of Hif1α (Huang et al. 1998), confirmed the importance of the identified HRE in the Sirt2 promoter for Hif1α-mediated repression of Sirt2 promoter activity (Fig. 4H,I). Lastly, when 3T3-L1-derived adipocytes were exposed to hypoxia (3% O_2) in the presence or absence of shHif1α and assessed for Sirt2 transcription, we observed hypoxia-induced, Hif1α-dependent, Sirt2 transcriptional repression (Supplemental Material; Supplemental Fig. 4I). In sum, these results identify *Sirt2* as a novel Hif1α-repressed target gene.

Pgc1α is a potential deacetylation target of Sirt2

The results above suggest a role for Sirt2 (via Pgc1α) in mediating the increase in FAO upon Hif1α inactivation. To demonstrate a relevance of the Hif1α–Sirt2–Pgc1α axis in adipocyte metabolism, we addressed the impact of shRNA-mediated knockdown of Hif1α, Sirt1, Sirt2, or combinations thereof in differentiated 3T3-L1-derived adipocytes and assessed FAO using the Seahorse Bioscience 24XF extracellular flux analyzer. While knockdown of Sirt2 alone significantly inhibited adipocyte FAO, Sirt1 knockdown did not. Similarly, on the background of Hif1α inactivation, knockdown of Sirt2 dramatically repressed Hif1α inactivation-mediated FAO induction (Fig. 5A). Knockdown of Sirt1 failed to significantly repress Hif1α

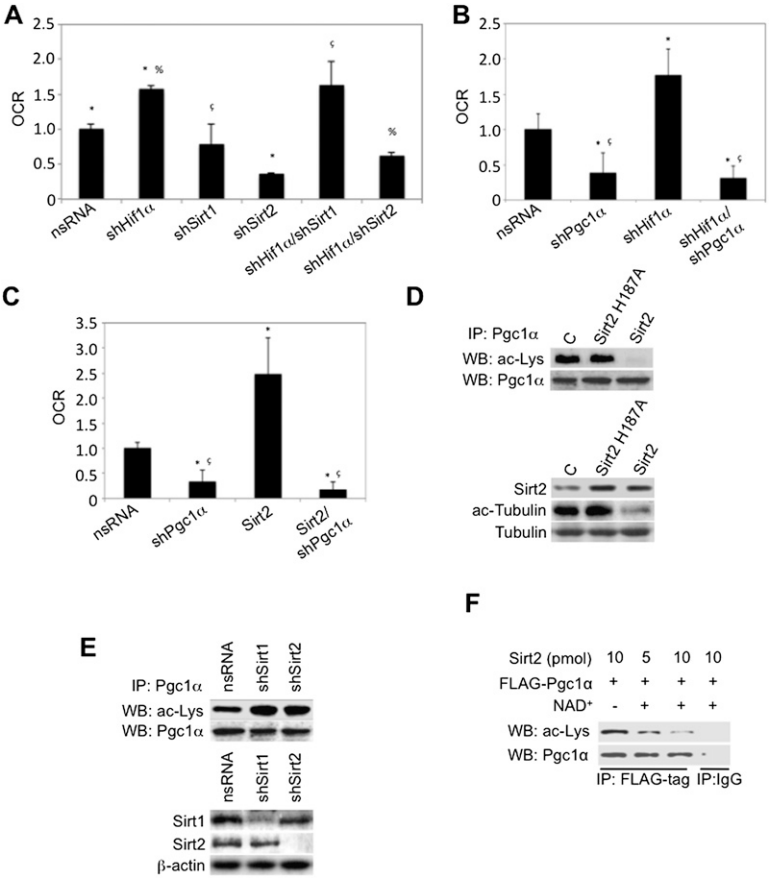

Figure 5. Sirt2 promotes oxidative catabolism via Pgc1α deacetylation. (*A*) 3T3-L1-derived adipocytes were infected with empty nsRNA, shHif1α, shSirt1, shSirt2, or a combination thereof and assessed for oleate-induced oxygen consumption as a measure of fatty acid β-oxidation using the Seahorse Bioscience 24XF extracellular flux analyzer. The normalized OCR is shown. (*) $P < 0.01$ compared with control nsRNA, set at 1.0; (%) $P < 0.01$ compared with shHif1α; (ç) $P < 0.01$ compared with shSirt1. Data are mean ± SEM of values from each group. (*B*) 3T3-L1-derived adipocytes were infected with empty nsRNA, shPgc1α, shHif1α, or shHif1α/shPgc1α and assessed for oleate-induced oxygen consumption as a measure of fatty acid β-oxidation using the Seahorse Bioscience 24XF extracellular flux analyzer. The normalized OCR is shown. (*) $P < 0.01$ compared with control nsRNA, set at 1.0; (ç) $P < 0.01$ compared with shHif1α. Data are mean ± SEM of values from each group. (*C*) Lentivirus-mediated ectopic expression of Sirt2 was performed in 3T3-L1-derived adipocytes in the presence or absence of shPgc1α and assessed for oleate-induced oxygen consumption as a measure of fatty acid β-oxidation using the Seahorse Bioscience 24XF extracellular flux analyzer. The normalized OCR is shown. (*) $P < 0.01$ compared with control nsRNA, set at 1.0; (ç) $P < 0.01$ compared with Sirt2. Data are mean ± SEM of values from each group. (*D*, *top* panels) Ectopic lentiviral-mediated Sirt2 or Sirt2 H187A expression was performed in 293 cells, and lysates were immunoprecipitated with the Pgc1α antibody and probed for lysine acetylation and Pgc1α by immunoblotting. (*Bottom* panels) In parallel, lysates were probed for Sirt2 expression and tubulin acetylation by immunoblotting. (*E*, *top* panels) Lentiviral shRNA-mediated Sirt1 and Sirt2 knockdown was performed in 293 cells, and lysates were immunoprecipitated with the Pgc1α antibody and probed for lysine acetylation and Pgc1α by immunoblotting. (*Bottom* panels) In parallel, lysates were probed for Sirt1 and Sirt2 expression by immunoblotting. (*F*) Flag-tagged Pgc1α ectopically expressed in 293 cells was immunoprecipitated and incubated in the presence of varying amounts of purified Sirt2 protein in the presence or absence of NAD^+ as indicated and probed by immunoblotting for acetylated lysine and Pgc1α. Immunoprecipitation with IgG serves as a negative control.

inactivation-induced FAO (Fig. 5A). These results point to a key role for Sirt2 (but not of Sirt1) in the regulation of adipocyte FAO. Similarly, the effect of shRNA-mediated Pgc1α knockdown on the background of Hif1α inactivation or ectopic Sirt2 expression on adipocyte FAO capacity was determined. 3T3-L1 adipocytes were infected with lentiviruses encoding nsRNA, shHif1α, shPgc1α, shSirt2, or a combination thereof and assessed for FAO. Interestingly, the knockdown of Pgc1α proved sufficient to negate the FAO-inducing properties of both Hif1α inactivation and ectopic Sirt2 expression (Fig. 5B,C). These data therefore implicate the Hif1α–Sirt2–Pgc1α axis in regulating adipocyte FAO.

However, as the validity of this axis is dependent on the capacity for Sirt2 to directly deacetylate Pgc1α, we examined whether Pgc1α is a Sirt2 target protein. To this end, wild-type Sirt2 or a deacetylase mutant of Sirt2 (Sirt2 H187A) (Finnin et al. 2001) was ectopically expressed in 293 embryonic kidney cancer cells and assayed for endogenous Pgc1α deacetylation. Sirt2 expression prompted the deacetylation of Pgc1α (Fig. 5D, top panel) and tubulin (Fig. 5D, bottom panel), while ectopic expression of Sirt2 H187A did not significantly impact the acetylation state of Pgc1α or tubulin (Fig. 5D). Conversely, shRNA-mediated depletion of Sirt2 resulted in elevated levels of Pgc1α acetylation compared with controls (Fig. 5E). Depletion of Sirt1 similarly led to increased levels of Pgc1α acetylation (Fig. 5E), implying that in these cancer cells, both Sirt2 and Sirt1 contribute to Pgc1α acetylation. The efficacy of Sirt2 overexpression or knockdown, Pgc1α knockdown, and the specificity of the Pgc1α antibody used for immunoprecipitation was verified by immunoblotting and/or immunoprecipitation (Supplemental Material; Supplemental Fig. 5A–E). Finally, incubation of anti-Flag-Pgc1α immunoprecipitates from 293 cells with increasing amounts of bacterial-purified Sirt2 caused a dose- and NAD^+-dependent deacetylation of Pgc1α in this in vitro assay (Fig. 5F). Taken together, these findings support the view that Pgc1α represents a novel substrate of Sirt2 whose acetylation state is regulated, at least in part, by Hif1α via transcriptional suppression of *Sirt2* and suggests a key role for Sirt2 and Pgc1α as downstream mediators of the negative effects of Hif1α on FAO capacity in adipocytes.

HIF1α and SIRT2 expression inversely correlates in human and mouse obesity

Given the functional relationship between Hif1α and Sirt2 suppression in mouse dietary obesity, we assessed visceral adipose biopsies of obese human subjects (body mass index [BMI] > 30.0 kg/m^2) with defects in glucose homeostasis for HIF1α, SIRT2, and CPT1 protein expression and mRNA expression of FAO regulators (Fig. 6A–D; Supplemental Material; Supplemental Table 1). Specificity of the SIRT2 antibody was verified by immunoblotting (Supplemental Material; Supplemental Fig. 6A). Lean subjects (BMI < 25.0 kg/m^2) were generally characterized by low HIF1α and high SIRT2 and CPT1 protein levels, while the inverse was observed in biopsies of obese subjects (Fig. 6D). Moreover, an overall decrease in the expression of FAO regulators was noted in adipose tissue of obese versus lean subjects (Fig. 6C,D). Importantly, the inverse correlation between HIF1α and SIRT2 is recapitulated in a mouse model of diet-induced obesity and defective glucose homeostasis (Supplemental Material; Supplemental Figs. 2K, 6B,C). Consistent with the increased expression of mitochondrial biogenesis regulators and of components of the mitochondrial electron transport chain upon Hif1α inactivation in WAT of mice maintained on a HFD, visceral WAT biopsies of lean human subjects revealed increased expression of such factors, indicative of greater mitochondrial biogenesis and activity compared with obese subjects (Fig. 6E). Thus, HIF1α-mediated repression of SIRT2 expression and activity, and the consequent inhibition of mitochondrial lipid catabolism in white adipocytes, may represent a potential contributing component in human obesity.

Discussion

Here we demonstrate a key role of Hif1α in the initiation and preservation of diet-induced obesity in part through direct transcriptional repression of Sirt2 NAD$^+$-dependent deacetylase. Moreover, we identify Pgc1α as a potential

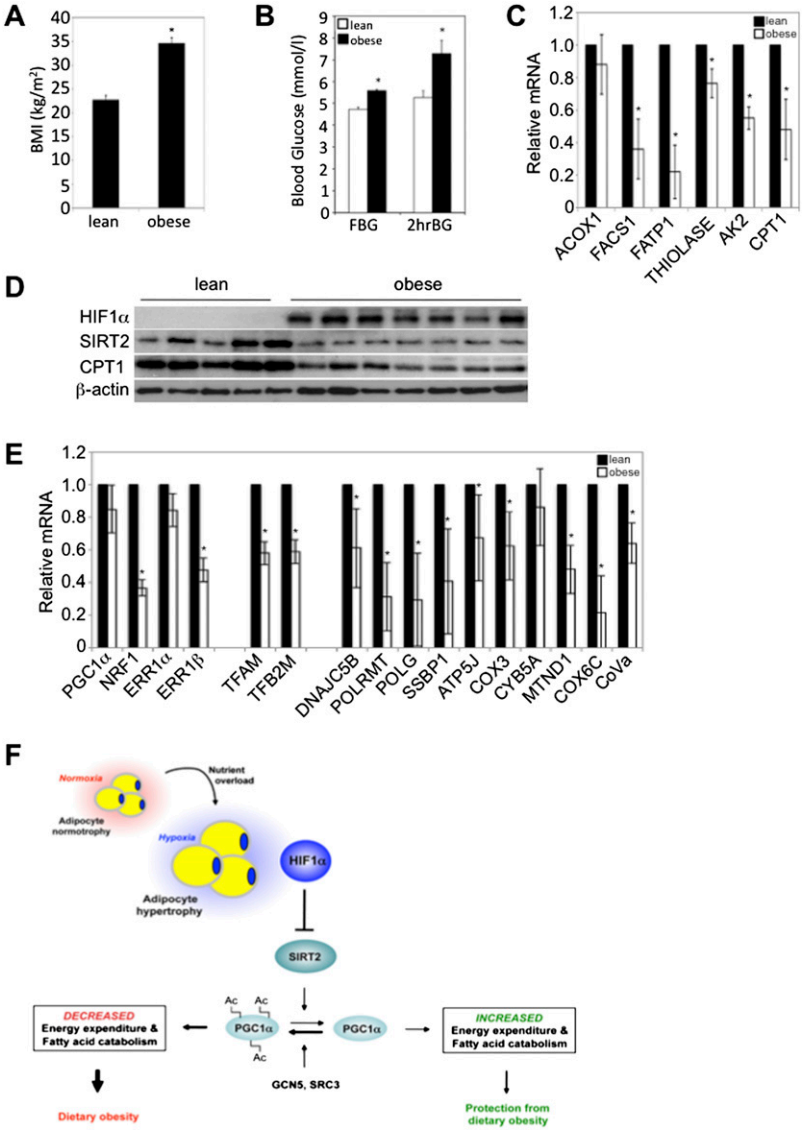

Figure 6. Sirt2 is down-regulated in human obesity. (*A*) Average BMI of subjects within the lean ($n = 9$) and obese ($n = 9$) groups, respectively. (*) $P < 0.01$ versus lean subjects. Data are mean ± SEM of values from each group. (*B*) Fasting (FBG) and 2-h oral GTT (2hrBG) blood glucose indices of the lean ($n = 9$) and obese ($n = 9$) groups are shown. (*) $P < 0.05$ versus lean subjects. Data are mean ± SEM of values from each group. (*C*) Gene expression profiling of visceral WAT biopsies of lean and obese subjects for components of FAO. All values were normalized internally to 18S RNA expression and to the lean samples, respectively. (*) $P < 0.05$ versus lean subjects. Data are mean ± SEM of values from the respective groups. (*D*) Visceral WAT biopsies of human lean or obese subjects were assessed for HIF1α, SIRT2, and CPT1 protein expression. β-Actin served as a loading control. (*E*) Gene expression profiling of visceral WAT biopsies of lean and obese subjects for regulators mitochondrial biogenesis and of mitochondrial complex and electron transport chain proteins. All values were normalized internally to 18S RNA expression and to the lean samples, respectively. (*) $P < 0.05$ versus lean subjects. Data are mean ± SEM of values from the respective groups. (*F*) Schematic representation of the transcriptional and enzymatic coregulation of SIRT2 by HIF1α. Nutrient overload-induced adipose expansion augments intra-adipose hypoxia, leading to adipocyte HIF1α accumulation. HIF1α represses SIRT2 transcription via interaction at a cross-species conserved HRE on the SIRT2 promoter. The repression of SIRT2 activity by HIF1α is predicted to support the maintenance of general control of amino acid synthesis, yeast, homolog-like 2 (GCN5/KAT2A)-mediated, and/or steroid receptor coactivator protein 3 (SRC3/NCOA3)-mediated Pgc1α hyperacetylation and its consequent inactivation, culminating in the maintenance of lipid anabolism and pathological adipose expansion. For additional details, see the text.

substrate of Sirt2. Accordingly, repression of Sirt2 by Hif1α in dietary obesity results in increased acetylation and Pgc1α inactivation. This creates a metabolic state of reduced FAO in adipocytes. The mechanistic relationship between pathologic adipose tissue mass expansion-associated Hif1α accumulation, Sirt2 suppression, and Pgc1α hyperacetylation is underscored by the observation that HIF1α protein levels in human obese subjects inversely correlate with protein levels of SIRT2 and CPT1, the rate-limiting enzyme in mitochondrial FAO. Hence, our findings support a model wherein adipose tissue hypoxia-induced Hif1α activation suppresses the Sirt2-NAD^+ metabolic regulatory system, leading to reduced oxidative lipid catabolism and mitochondrial biogenesis mediated in part through the inhibition of Pgc1α activity. This, in turn, facilitates lipid anabolism, white adipose mass expansion, and the development of obesity-associated pathologies, including glucose intolerance, insulin resistance, and diabetic cardiomyopathy (Fig. 6F).

Our observations link Hif1α activation to the suppression of adipocyte lipid catabolism. Strikingly, the effects of Hif1α on lipid catabolism are depot-specific and affect visceral but not subcutaneous fat. This is remarkable, considering that subcutaneous adipocytes are associated with greater lineage plasticity than visceral adipocytes (Cinti 2009). On the other hand, the observed Hif1α depot specificity may relate to the fact that visceral adipocytes are subjected to a greater degree of hypoxia and adipose tissue hypoperfusion than subcutaneous WAT (Gealekman et al. 2011), thus possibly hypersensitizing visceral WAT to tissue and adipocyte hypertrophy-induced hypoxia. Based on our data, it is possible that Hif1α inactivation promotes a brown adipocyte-like phenotype in visceral adipocytes through its capacity to induce mitochondrial biogenesis and function.

Mechanistically, our work unveiled that the Hif1α-dependent effects on adipocyte lipid catabolism are mediated through regulation of the sirtuin–Pgc1α system. Hif1α inhibits Sirt2 gene transcription via interaction at a cross-species conserved HRE on the *Sirt2* promoter. Although predominantly associated with transcriptional activation, recent reports have demonstrated Hif1α-mediated transcriptional repression (Eltzschig et al. 2005; Wang et al. 2009). The identification of Sirt2 as a downstream effector repressed by Hif1α therefore links dietary obesity-associated adipose tissue hypoxia and Hif1α activation to the inhibition of adipocyte-instrinsic pathways controlling FAO and energy expenditure.

Sirt2 is the most prominently expressed sirtuin family member in adipocytes (Jing et al. 2007; Wang et al. 2007). It was originally identified as a tubulin deacetylase. However, existing data suggest that Sirt2 is localized to both the nuclear and cytoplasmic compartment, implying that, in addition to tubulin, Sirt2 can target nuclear proteins for deacetylation. The fact that we detected significantly less acetylated Pgc1α in adipocytes deficient for Hif1α and that Sirt2 can deacetylate Pgc1α in vivo and in vitro suggests that Pgc1α may represent a nuclear substrate of Sirt2. Consistent with this, we found that Sirt2 predominantly localized to the nucleus in adipocytes. Pgc1α has been prominently associated with the regulation of the FAO gene program and energy expenditure (Handschin and Spiegelman 2006). Interestingly, its acetylation state has been reported to be critical in regulating its activity, such that hyperacetylation is associated with reduced Pgc1α coactivator function. Indeed, key Pgc1α-responsive promoters are negatively affected by Hif1α activation in a Sirt2-dependent manner. The identification of Pgc1α as a Sirt2 substrate therefore suggests that Hif1α regulates adipocyte mitochondrial biogenesis and FAO, at least in part, by affecting Sirt2-mediated Pgc1α substrate acetylation state.

In conclusion, our work identifies Hif1α as a central regulator of adipocyte lipid catabolism and energy expenditure. Hif1α mediates these effects, at least in part, by interfering with the function of the Sirt2, thereby creating a metabolic state permissive for the development of obesity in the face of nutrient overload. Since adipose HIF1α accumulation in human obese subjects correlates with low SIRT2, augmenting the activity of the SIRT2 pathway may represent a therapeutic approach for the treatment of obesity in humans.

Materials and methods

Human obesity studies

The human obesity study and clinical parameters documented in Supplemental Table 1 were performed as previously described (Tkacova et al. 2010). The study was approved by the Ethics Committee of the Derer's University Hospital, Slovak Health Care University in Bratislava, and conforms to the ethical guidelines of the 2000 Helsinki declaration. All patients and healthy control volunteers provided witnessed written informed consent before entry into the study.

Animal breeding and maintenance

Hif1α fl/fl mice were obtained from Randall S. Johnson (University of California at San Diego, San Diego, USA). The Fabp4/aP2-ERT2-cre/+ line was kindly provided by Daniel Metzger (CNRS, France). Leslie P. Kozak (Pennington Biomedical Research Center, Baton Rouge, LA, USA) generously provided the UCP1-cre/+ line. Primers used for mouse genotyping are listed in the Supplemental Material (Supplemental Table 2). The data represent studies with male mice, maintained at the RCHCI, ETH-Zurich, specific pathogen-free facility. Maintenance and animal experimentation were in accordance with the Swiss Federal Veterinary Office (BVET) guidelines.

Acknowledgments

We thank all members of the laboratory, especially P. Gerber, K. Eckhardt, S. Georgiev, and M. Duda. We are particularly grateful to N. Fankhauser for scientific help and advice. We are indebted to F. von Meyenn and M. Stoffel (ETH-Zurich, Switzerland) for equipment access. We thank A. Mitkova, R. Imrich, M. Vlcek, T. Kurdiova, and M. Balaz (Slovak Academy of Sciences, Slovakia), as well as V. Belan and M. Srbecky (Commenius University, Slovakia). Human obesity studies were supported by EC FP7 grants LipidomicNet (202272) and COST FA0602.

References

Black JC, Mosley A, Kitada T, Washburn M, Carey M. 2008. The SIRT2 deacetylase regulates autoacetylation of p300. *Mol Cell* **32:** 449–455.

Boudina S, Abel ED. 2010. Diabetic cardiomyopathy, causes and effects. *Rev Endocr Metab Disord* **11:** 31–39.

Buettner R, Parhofer KG, Woenckhaus M, Wrede CE, Kunz-Schughart LA, Scholmerich J, Bollheimer LC. 2006. Defining high-fat-diet rat models: Metabolic and molecular effects of different fat types. *J Mol Endocrinol* **36:** 485–501.

Cinti S. 2009. Transdifferentiation properties of adipocytes in the adipose organ. *Am J Physiol* **297:** E977–E986. doi: 10.1152/ajpendo.00183.2009.

Donohoe CL, Doyle SL, Reynolds JV. 2011. Visceral adiposity, insulin resistance and cancer risk. *Diabetol Metab Syndr* **3:** 12. doi: 10.1186/1758-5996-3-12.

Eltzschig HK, Abdulla P, Hoffman E, Hamilton KE, Daniels D, Schonfeld C, Loffler M, Reyes G, Duszenko M, Karhausen J, et al. 2005. HIF-1-dependent repression of equilibrative nucleoside transporter (ENT) in hypoxia. *J Exp Med* **202:** 1493–1505.

Finnin MS, Donigian JR, Pavletich NP. 2001. Structure of the histone deacetylase SIRT2. *Nat Struct Biol* **8:** 621–625.

Gealekman O, Guseva N, Hartigan C, Apotheker S, Gorgoglione M, Gurav K, Tran KV, Straubhaar J, Nicoloro S, Czech MP, et al. 2011. Depot-specific differences and insufficient subcutaneous adipose tissue angiogenesis in human obesity. *Circulation* **123:** 186–194.

Guerra C, Navarro P, Valverde AM, Arribas M, Bruning J, Kozak LP, Kahn CR, Benito M. 2001. Brown adipose tissue-specific insulin receptor knockout shows diabetic phenotype without insulin resistance. *J Clin Invest* **108:** 1205–1213.

Halberg N, Khan T, Trujillo ME, Wernstedt-Asterholm I, Attie AD, Sherwani S, Wang ZV, Landskroner-Eiger S, Dineen S, Magalang UJ, et al. 2009. Hypoxia-inducible factor 1α induces fibrosis and insulin resistance in white adipose tissue. *Mol Cell Biol* **29:** 4467–4483.

Handschin C, Spiegelman BM. 2006. Peroxisome proliferator-activated receptor γ coactivator 1 coactivators, energy homeostasis, and metabolism. *Endocr Rev* **27:** 728–735.

Hu CJ, Wang LY, Chodosh LA, Keith B, Simon MC. 2003. Differential roles of hypoxia-inducible factor 1α (HIF-1α) and HIF-2α in hypoxic gene regulation. *Mol Cell Biol* **23:** 9361–9374.

Huang LE, Gu J, Schau M, Bunn HF. 1998. Regulation of hypoxia-inducible factor 1α is mediated by an O_2-dependent degradation domain via the ubiquitin–proteasome pathway. *Proc Natl Acad Sci* **95:** 7987–7992.

Imagawa M, Tsuchiya T, Nishihara T. 1999. Identification of inducible genes at the early stage of adipocyte differentiation of 3T3-L1 cells. *Biochem Biophys Res Commun* **254:** 299–305.

Imai T, Jiang M, Chambon P, Metzger D. 2001. Impaired adipogenesis and lipolysis in the mouse upon selective ablation of the retinoid X receptor α mediated by a tamoxifen-inducible chimeric Cre recombinase (Cre-ERT2) in adipocytes. *Proc Natl Acad Sci* **98:** 224–228.

Jiang C, Qu A, Matsubara T, Chanturiya T, Jou W, Gavrilova O, Shah YM, Gonzalez FJ. 2011. Disruption of hypoxia-inducible factor 1 in adipocytes improves insulin sensitivity and decreases adiposity in high-fat diet-fed mice. *Diabetes* **60:** 2484–2495.

Jing E, Gesta S, Kahn CR. 2007. SIRT2 regulates adipocyte differentiation through FoxO1 acetylation/deacetylation. *Cell Metab* **6:** 105–114.

Kaelin WG Jr, Ratcliffe PJ. 2008. Oxygen sensing by metazoans: The central role of the HIF hydroxylase pathway. *Mol Cell* **30:** 393–402.

Kopecky J, Rossmeisl M, Flachs P, Brauner P, Sponarova J, Matejkova O, Prazak T, Ruzickova J, Bardova K, Kuda O. 2004. Energy metabolism of adipose tissue–physiological aspects and target in obesity treatment. *Physiol Res* **53:** S225–S232.

Krishnan J, Suter M, Windak R, Krebs T, Felley A, Montessuit C, Tokarska-Schlattner M, Aasum E, Bogdanova A, Perriard E, et al. 2009. Activation of a HIF1α-PPARγ axis underlies the integration of glycolytic and lipid anabolic pathways in pathologic cardiac hypertrophy. *Cell Metab* **9:** 512–524.

Martens K, Bottelbergs A, Baes M. 2010. Ectopic recombination in the central and peripheral nervous system by aP2/FABP4-Cre mice: Implications for metabolism research. *FEBS Lett* **584:** 1054–1058.

Montague CT, O'Rahilly S. 2000. The perils of portliness: Causes and consequences of visceral adiposity. *Diabetes* **49:** 883–888.

North BJ, Verdin E. 2004. Sirtuins: Sir2-related NAD-dependent protein deacetylases. *Genome Biol* **5:** 224. doi: 10.1186/gb-2004-5-5-224.

North BJ, Marshall BL, Borra MT, Denu JM, Verdin E. 2003. The human Sir2 ortholog, SIRT2, is an NAD^+-dependent tubulin deacetylase. *Mol Cell* **11:** 437–444.

Nunn JF. 1972. Nomograms for calculation of oxygen consumption and respiratory exchange ratio. *BMJ* **4:** 18–20.

Rodgers JT, Lerin C, Haas W, Gygi SP, Spiegelman BM, Puigserver P. 2005. Nutrient control of glucose homeostasis through a complex of PGC-1α and SIRT1. *Nature* **434:** 113–118.

Tkacova R, Ukropec J, Skyba P, Ukropcova B, Pobeha P, Kurdiova T, Joppa P, Klimes I, Tkac I, Gasperikova D. 2010. Increased adipose tissue expression of proinflammatory CD40, MKK4 and JNK in patients with very severe chronic obstructive pulmonary disease. *Respiration* **81:** 386–393.

Urs S, Harrington A, Liaw L, Small D. 2006. Selective expression of an aP2/fatty acid binding protein 4-Cre transgene in non-adipogenic tissues during embryonic development. *Transgenic Res* **15:** 647–653.

Vague J. 1947. La différénciation sexuelle, facteur determinant des formes de l'obésité. *Presse Med* **55:** 339–340.

van der Kuip M, de Meer K, Oosterveld MJ, Lafeber HN, Gemke RJ. 2004. Simple and accurate assessment of energy expenditure in ventilated paediatric intensive care patients. *Clin Nutr* **23:** 657–663.

Wang F, Nguyen M, Qin FX, Tong Q. 2007. SIRT2 deacetylates FOXO3a in response to oxidative stress and caloric restriction. *Aging Cell* **6:** 505–514.

Wang Y, Roche O, Yan MS, Finak G, Evans AJ, Metcalf JL, Hast BE, Hanna SC, Wondergem B, Furge KA, et al. 2009. Regulation of endocytosis via the oxygen-sensing pathway. *Nat Med* **15:** 319–324.

Wellen KE, Thompson CB. 2010. Cellular metabolic stress: Considering how cells respond to nutrient excess. *Mol Cell* **40:** 323–332.

Wood IS, de Heredia FP, Wang B, Trayhurn P. 2009. Cellular hypoxia and adipose tissue dysfunction in obesity. *Proc Nutr Soc* **68:** 370–377.

Wu Z, Puigserver P, Andersson U, Zhang C, Adelmant G, Mootha V, Troy A, Cinti S, Lowell B, Scarpulla RC, et al. 1999. Mechanisms controlling mitochondrial biogenesis and respiration through the thermogenic coactivator PGC-1. *Cell* **98:** 115–124.

Ye J. 2009. Emerging role of adipose tissue hypoxia in obesity and insulin resistance. *Int J Obes (Lond)* **33:** 54–66.

Ye J, Gao Z, Yin J, He Q. 2007. Hypoxia is a potential risk factor for chronic inflammation and adiponectin reduction in adipose tissue of ob/ob and dietary obese mice. *Am J Physiol* **293:** E1118–E1128. doi: 10.1152/ajpendo.00435.2007.

Zhang X, Lam KS, Ye H, Chung SK, Zhou M, Wang Y, Xu A. 2010. Adipose tissue-specific inhibition of hypoxia-inducible factor 1α induces obesity and glucose intolerance by impeding energy expenditure in mice. *J Biol Chem* **285:** 32869–32877.